Effects of mountains on aerosols determined by AERONET/DRAGON/J-ALPS measurements and regional model simulations

Makiko Nakata[1], Mizuo Kajino[2], and Yousuke Sato[3]

[1] Faculty of Applied sociology, Kindai University, Japan.

[2] Meteorological Research Institute, Japan.

[3] Faculty of Science, Hokkaido University, Japan.

Corresponding author: Makiko Nakata (nakata@socio.kindai.ac.jp)

Key Points:

- To investigate the effect of mountains on aerosols, a regional model was implemented for field campaign over a Japanese mountain region.
- This study found that mountains have a blocking effect on advection aerosols, but also increase aerosol concentrations in basins.
- The J-ALPS sites showed that the mountain effect prevented external advection, even on days with widespread transboundary pollution.

Abstract

The NASA/AERONET field campaign DRAGON/J-ALPS (Distributed Regional Aerosol Gridded Observation Networks/Joint work to the AerosoL Properties and Process Simulations) was conducted from March 2020 to May 2021 in Nagano, Japan. Twelve sun photometers were installed around Nagano prefecture. The effects of topography on aerosols were studied using observations and simulations. In this study, a regional chemical transport model (SCALE-Chem) was employed. Three numerical experiments were conducted: E1 (control experiment), E2 (E1 without topography), and E3 (E1 with removal of all anthropogenic emissions over Nagano prefecture). In E2, the terrain effect was not considered; the difference between E1 and E2 indicated the influence of mountains. The differences between E1 and E3 evaluate the local emission effect. In some cases, the mountainous terrain seemed to have suppressed aerosol inflow (i.e., reduced aerosol concentration), while in other cases, the mountains contributed to aerosol retention on days when aerosols tended to accumulate in mountain basins due to local emissions. Thus, while mountains prevent the inflow of aerosols from outside, they also contribute to increased aerosol concentration in the basin. Naturally, more significant effects are produced by meteorological conditions and the presence or absence of transboundary pollution from the outside. From observations and model simulations, we found that the aerosol concentration was not high around the J-ALPS site because of the mountain effect that prevents advection from the outside, even when transboundary pollution was observed in Japan in March 2020.

Plain Language Summary

Aerosol observations by the NASA/AERONET field campaign were conducted in the mountainous regions of Japan from March 2020 to May 2021. This field campaign is called DRAGON/J-ALPS because the target area includes the mountains known as the Japanese Alps. In this study, we investigated how mountains affect aerosol distribution by using simulations with the regional chemical transport model SCALE-Chem in conjunction with observational data in mountainous regions. To investigate the effect of mountains, simulations were conducted with and without mountains. In addition, to investigate the effect of local sources, we compared simulations with and without anthropogenic emissions in the target area. The simulation results showed that the mountains blocked aerosols and created a basin effect by increasing the aerosol concentration near the surface. Furthermore, averaged throughout March 2020, the effect of the mountains blocking aerosols was greater than the effect of the mountains increasing aerosol concentrations near the surface. This finding suggests that the blocking effect of the surrounding mountains prevented an increase in aerosol concentrations at the J-ALPS site even on days when transboundary pollution from mainland China arrived in Japan.

1 Introduction

Atmospheric aerosols are attracting attention not only as substances that affect the climate (IPCC, 2013) but also as $PM_{2.5}$, which causes air pollution (Shinder et al., 2016, Van Donkelaar et al., 2015). Because aerosols are not uniform and have a local spatio-temporal distribution, high spatial resolution observations are very important. The AErosol RObotic NETwork project (AERONET; Holben et al., 1998) is an international network of ground-based sun photometers

that provides atmospheric aerosol properties. The series of distributed regional aerosol gridded observation network (DRAGON) campaigns began in 2011 as a relatively high spatial density of ground-based sun photometers and other associated measurements of limited duration (Holben et al., 2018). DRAGON field campaigns are conducted worldwide to provide high-resolution ground-based data for remote sensing and model simulations.

The following two campaigns, DRAGON-KOREA and DRAGON-JAPAN, operated from March to June 2012 to elucidate the aerosol characteristics of urban areas in East Asia where transboundary and urban pollution are mixed. During DRAGON-KOREA in Seoul, it was observed that industry and fossil fuel power generation contributed emissions to a significant pollution aerosol loading in addition to aerosols transported from mainland China. DRAGON-JAPAN was held mainly in Osaka during the DRAGON-KOREA campaign. In Osaka, small particles emitted from factories are dominant, but when yellow dust particles are introduced, the percentage of large particles increases (Nakata et al., 2015). Further measurements with a mobile sun photometer attached to a car showed that aerosol concentrations rapidly changed in time and space over most of the Osaka area (Sano et al., 2016). Thus, the East Asian region has been suffering from the effects of air pollution, much of which is transboundary. The extant literature reports a significant impact of transboundary air pollution in Japan (Aikawa et al., 2010; Kaneyasu et al., 2014; Nakata et al., 2015). Therefore, when considering the distribution of atmospheric aerosols in Japan, it is necessary to consider not only aerosols of local origin but also transboundary aerosols. Past DRAGON campaigns in Japan have focused on large urban areas and areas susceptible to transboundary pollution. How do aerosols behave in mountainous areas with complex topography? It has been reported that the mountainous areas of the Alps, where one would expect a clean air environment, are surprisingly polluted as pollutants emitted from the surrounding areas are carried by the wind through the valleys (Diemoz et al., 2019). Inspired by this report, DRAGON-JALPS was designed to observe the effects of mountain topography on aerosols in the mountainous areas of Japan.

Air pollutant emissions are the primary driver of the increase in aerosol concentration, and meteorological conditions play a major role in exacerbating air pollution (Hu et al., 2020). Because topography has a considerable effect on the meteorological conditions in the area, a study of the local terrain associated with weather patterns and pollutant transport is important (Chuang et al., 2008). The effects of topography on aerosol concentrations in East Asia have also been studied. The Sichuan Basin in Southwest China has frequent heavy pollution, and the topographic effects intensify haze pollution by reducing wind speed and varying air temperature and humidity in the lower troposphere (Shu et al., 2020; Zhang et al., 2019). A study of the Twain-Hu basin in Central China has shown that the basin topography plays an important role in the significant increase in $PM_{2.5}$, although the meteorology altered by topography can alleviate local $PM_{2.5}$ pollution over the basin (Hu et al., 2020). The simulation results show that topography has a considerable influence on haze pollution in Beijing (Zhang et al., 2018) and Taipei (Chuang et al., 2008).

The area around the Japanese Alps, which is the focus of this study, has a lower concentration of atmospheric aerosols than Osaka, which is also in Japan. We hypothesize that this may be due to the effect of the surrounding high mountains that mitigate transboundary pollution. The issue of transboundary pollution, where polluted air from Tokyo, a large city located east of Nagano Prefecture, travels over mountain passes and is transported to mountainous areas, has been dealt with observations and models (Chang et al., 1989; Sasaki et al., 1988). However, transboundary pollution from Tokyo is mainly observed in the summer season, and there are few

cases in the spring season, which is the target of this study. Rather, spring is the time when transboundary pollution from the Chinese mainland is most likely to occur. Therefore, the main objective of this study is to investigate the effect of mountains on long-distance transboundary pollution by taking advantage of the opportunity of the intensive field campaign of J-ALPS. We will clarify how the mountains affect the aerosol concentration by using ground-based observation data during the DRAGON-JALPS field campaign and simulated by a chemical transport model.

2 Materials and Methods

2.1 AERONET field campaign: J-ALPS

2.1.1 Target area

Nagano Prefecture, the target area of J-ALPS, is located at the center of Japan's main island and surrounded by mountains over 2000 m with multiple basins. These basins are located at altitudes of 350–700 m, and some of them are connected to each other by major rivers. The headwaters of all the major rivers are located in the prefecture, and because some head to the Sea of Japan and others to the Pacific Ocean, the area around some of the headwaters is a watershed in the central part of the main island of Japan. From the northwest to the south of the prefecture, there are three mountain ranges: the Hida, Kiso, and Akaishi Mountains, collectively known as the Japanese Alps (Togashi, 2001). The Hida, Kiso, and Akaishi Mountains are sometimes referred to as the Northern, Central, and Southern Japanese Alps, respectively.

Geographic information on the location and elevation of each J-ALPS site is shown in Fig.1 and Table 1. The altitude of each site is the height of the location where the sun photometer is installed. Both the Hakuba and Omachi sites are located in the northwestern part of Nagano Prefecture, at the foot of the Northern Japanese Alps, with mountains around 3,000 m high on the west side and mountains around 1,500 m high on the east side. Omachi city is to the south of Hakuba, as shown in Fig.1. The climate of both sites is cool in summer and cold in winter, with abundant snowfall. Matsumoto is a city with 200,000 people located slightly west of the center of Nagano Prefecture, in the middle of the Matsumoto Basin between two mountain ranges. The climate is characterized by diurnal and annual temperature differences, little precipitation, and many sunny days. Suwa is located in central Nagano Prefecture, bordered by Lake Suwa to the northwest and sandwiched between mountains to the west and east, roughly in the center of the Suwa Basin. The climate in Suwa is characterized by more precipitation in spring, summer, and autumn and far less precipitation in winter. The Minowa site is located in Minami-Minowa village in the southern part of Nagano Prefecture, and the Ina site is situated in Ina city in the south. Minowa and Ina lie in the northern part of the Ina Basin, with the Southern Japanese Alps to the east, the Central Japanese Alps to the west, and the Tenryū River running through the center of the basin. Iida is located in the southernmost part of Nagano Prefecture. The Iida basin, characterized by terraces developed on both sides of the Tenryū River and the fans formed by its tributaries, has a mild climate and relatively flat surfaces.

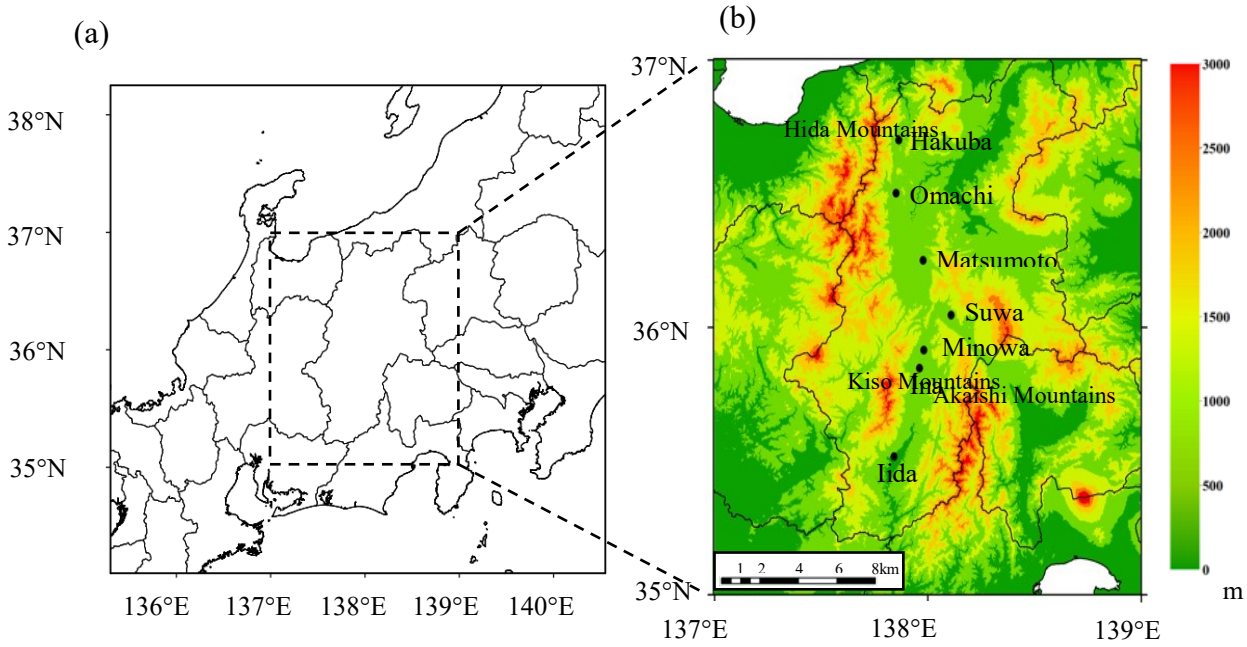

Figure 1. Geographic information of the model simulation (a) and the observation station of J-ALPS (b). The color scale on the right side denotes the elevation in meters.

Table 1. Specific geographic information of J-ALPS observation.

Site name	Latitude (degree)	Longitude (degree)	Altitude (m)
Hakuba	N 36.701	E 137.864	703
Omachi	N 36.503	E 137.851	751
Matsumoto	N 36.251	E 137.978	626
Suwa	N 36.046	E 138.109	766
Minowa	N 35.915	E 137.981	713
Ina	N 35.848	E 137.961	683
Iida	N 35.517	E 137.842	490

2.1.2 Measurements

A Cimel electric sun photometer was installed at each site in Fig.1 in March 2020. Sun photometer measurements of direct solar radiation provide information for calculating the columnar aerosol optical thickness (AOT). Aerosol optical thickness can be used to compute columnar water vapor and estimate the aerosol size distribution using the Ångström exponent relationship. We used version 3 of the AERONET database with an algorithm that provides fully automatic cloud screening and instrument anomaly quality control (Giles et al., 2009). The version 3 algorithm processing includes three quality levels. Level 1.0 data use the pre-field deployment sun calibration. Level 1.5 data use Level 1.0 data and apply cloud-screening and automatic quality control procedures. Data are raised to Level 2.0 after applying the final post-field deployment sun

calibration to Level 1.5 data. The Level 2 data is the most accurate, but it provides a longer delay due to the requirement of post-field final calibration, so we used the Level 1.5 data, which is the most accurate available. To determine the air quality near the ground, we used the $PM_{2.5}$ concentration data observed near the J-ALPS site. The Japanese Environment Ministry consolidates the network of air pollution monitoring, including sulfur dioxide, nitrogen dioxide, carbon monoxide, photochemical oxidants, suspended particulate matter, and $PM_{2.5}$, and provides the monitoring value by the Atmospheric Environmental Regional Observation System (AEROS: http://soramame.taiki.go.jp/). Since $PM_{2.5}$ concentrations are not observed near all J-ALPS sites, we used $PM_{2.5}$ concentration data only near the three sites in Matsumoto, Suwa, and Ina. Additionally, field observations were conducted in the Ina Basin on March 19 and 20, 2020, using portable sun photometers, a $PM_{2.5}$, and a ceilometer. The Microtops-2 portable sun photometer is easy to carry; it added to our fieldwork and provided AOT (Nakata et al. 2013; Sano et al., 2016). We used a Microtops-2 photometer, calibrated with a standard Aerosol Robotics Network-Cimel (AERONET-Cimel) radiometer. The P-Sensor $PM_{2.5}$, developed by the Nagoya University and Panasonic Corporation, uses the light scattering method. In addition, we used a compact and lightweight Vaisala ceilometer CL31, which can be used for cloud-base height and vertical visibility measurements.

3 Regional chemical transport model simulation: SCALE-Chem

3.1 Model description

In this study, a regional chemical transport model simulation was conducted to investigate the effects of terrain on aerosols. A chemical transport model (Kajino et al., 2019, 2021) was implemented in the Scalable Computing for Advanced Library and Environment (SCALE) meteorological model (Nishizawa et al., 2015; Sato et al., 2015). The chemical transport model consists of advection, turbulent diffusion, gas-phase photochemistry, SOA chemistry, liquid-phase chemistry, heterogeneous chemical reactions, and aerosol microphysical processes. The aerosol microphysical processes include new particle formation, surface equilibrium vapor pressures of organic and inorganic compounds, condensation and evaporation, Brownian coagulation, dry deposition, grid-scale in-cloud scavenging, grid-scale below-cloud scavenging, sub-grid scale convection and scavenging, and fog deposition processes. The aerosol categories are Aitken, soot-free accumulation, accumulation internally mixed with soot, dust, and sea salt. The model considers 12 tracers including two moments (0th (number) and 2nd (proportional to surface area)) and a mass of ten components (unidentified mass, or anthropogenic dust(UID), black carbon (BC), organic mass (OM), mineral dust (MD), non-volatile components of sea salt (NS), SO_4^{2-}, NO_3^-, NH_4^+, Cl^-, and H_2O) for each category. We used a chemical transport model coupled offline to SCALE (SCALE-Chem). Offline coupling is a method in which a meteorological simulation is first performed, and then the results are used to simulate chemical transport. A meteorological simulation is required only once for an offline coupling model. Therefore, offline simulations are computationally more efficient during sensitivity simulations (Kajno et al., 2019). Figure 1 shows the simulation domain, which covers the central region of Japan with 92 × 92 horizontal grid cells with a grid resolution of 5 km and 5 km in latitude and longitude, respectively. First, a meteorological simulation was performed by SCALE. A mesoscale analysis (MANL) produced by the Japan Meteorological Agency (JMA) was used for the initial and boundary conditions of the SCALE. Surface heights based on GTOPO 30 from the United States Geological Survey The

target period was March 2020, and we simulated the period from March 1 to 23, including March 19 and 20, when we conducted on-site observations. A single run by SCALE started at 0:00 Coordinated Universal Time (UTC) on a date in the period and stopped after 30 h and 6 h from the initial time was discarded as the spin-up (Inatsu et al., 2020). The boundary conditions for the chemical transport model were built by serially connecting the outputs of the everyday runs. REASv2 (Kurokawa et al. 2013) for anthropogenic emissions with monthly variations, and the method of Li et al. (2017) was used for the hourly and vertical profiles of the emissions. We used the monthly Global Fire Emissions Database (GFED3; Giglio et al. 2010) for open biomass burning emissions and the Model of Emissions of Gases and Aerosols from Nature (MEGAN2; Guenther et al.2006) for biogenic emissions. Hourly volcanic SO_2 emissions in Japan developed by Kajino et al. (2021) were used. For the nesting boundary condition, we used the 3-D concentration over the Asian region calculated by NHM-Chem with the same model domain (covering East Asia with 30 km grid resolutions) and the same emission inventories as Kajino et al. (2019). The simulated $PM_{2.5}$ was derived as a proportion of the dry mass in which the aerodynamic ambient (wet) diameter was smaller than 2.5 μm. The Mie theory calculation was performed to derive the AOT at a wavelength of 500 nm using simulated log-normal size distribution parameters and chemical compositions.

To investigate the terrain effects on aerosols around J-ALPS sites, three numerical experiments, E1 (control experiment), E2 (E1 without topography), and E3 (E1 with removal all anthropogenic emissions over Nagano prefecture), were evaluated. The differences between E1 and E2 represent the impact of topography on aerosols. For E2, the meteorological simulation was performed without topography; that is, the region was flat. The same meteorological simulation result from the SCALE was used for E1 and E3. Then, E1 minus E3 evaluated the local anthropogenic emission effect on the aerosols.

3.2 Validation of the measurements

The simulation results of the E1-experiment by SCALE-Chem, described in the previous section and abbreviated as E1 hereafter, were compared with observed AOT at J-ALPS sites. Figure 2 presents the daily mean AOT (500) at a wavelength of 500 nm at six J-ALPS sites (Hakuba, Omachi, Matsumoto, Suwa, Minowa, and Iida in Fig.2 (a) to Fig. (f), respectively). The solid curve denotes the simulated results obtained using SCALE-Chem. The dots show AERONET Level 1.5 data at the J-ALPS sites. It is clear from Fig. 2 that the amount of data varies from site to site because the data acquisition period varies depending on the installation conditions of the equipment and weather conditions. Sun photometry cannot obtain data on cloudy or rainy days. For example, the Minowa site was unable to obtain data in the latter half of March, while the Matsumoto site was only able to obtain data for the last few days of the target period. Further observation data were not available at the Ina site in March 2020. Then, because the amount of data was too small to examine the correlation between the model and observed data for each site, six sites were averaged to examine the correlation of daily changes between the model simulations and measurements (Fig.2 (g)). The daily average value of the AERONET data showed that AOT (500) exceeding 0.3 was observed in Matsumoto, Suwa, and Iida on March 22, 2020, but no high aerosol concentration event with AOT exceeding 0.5 was observed, indicating that the AOT (500) at the J-ALPS site was low. A comparison of the average values for each site in Fig.2 (h) showed that the AOT (500) values at Matsumoto tended to be the highest in the measurements and model simulations. Figure 2 shows that the SCALE-Chem simulation results reproduce the AOT (500) values observed at the AERONET/J-ALPS site.

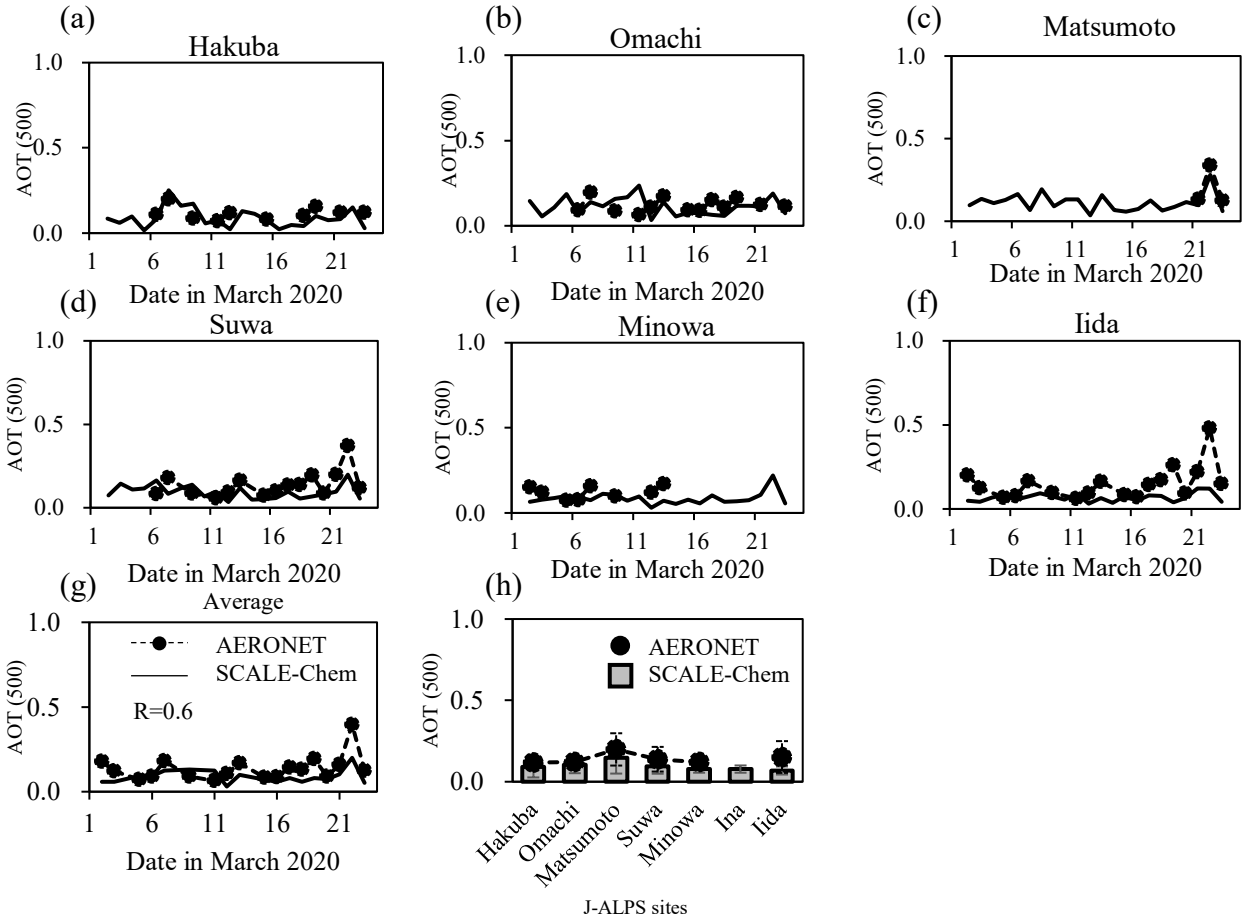

Figure 2. Daily mean AOT (500) at six J-ALPS sites as Hakuba, Omachi, Matsumoto, Suwa, Minowa, and Iida in Fig. (a) to Fig. (f), respectively. The solid curve denotes the simulated results by SCALE-Chem. The dots show AERONET Level 1.5 data at J-ALPS sites. Figs. (h) and (g) represent the AOT (500) values averaging over six sites and over the observation days, respectively.

Since AEROS observations of $PM_{2.5}$ concentrations were made near the Matsumoto, Suwa, and Ina sites of the J-ALPS, we compared the model results with the data shown in Fig. 3. The $PM_{2.5}$ concentrations were also not very high, but as with AOT, the trend of higher concentrations on March 22 was simulated in the model. The simulated concentrations at the three sites were underestimated, and this trend was more pronounced at the Matsumoto site. The Matsumoto site is located in the urban area of Matsumoto City, and there are potential problems with the uncertainty of the inventory and the spatial representativeness of the observation sites.

The results of observations in the Ina Basin using portable instruments were also compared with the model. The observation site is located between the Ina and Minowa sites and along the Tenryū River at (N35.878°, E137.988°) and at an altitude of 670 m. Observations were conducted at the site on March 19 and 20, 2020. The $PM_{2.5}$ concentration levels in the observed area were usually not too high, with an annual average value of ~10 $\mu g/m^3$. However, the morning of March 19 showed higher than usual values of $PM_{2.5}$, whereas, on March 20, lower than usual values were

observed. Additional measurements were performed using portable sun photometers. The Microtops-2 instrument detected a high AOT on the morning of March 19 and a low AOT on March 20. These features were consistent with the ceilometer measurements. Notably, the ceilometer measured the vertical distribution of atmospheric aerosols. The measurements recorded on March 19, 2020, showed high concentrations of air pollutants in the morning. Figure 4 shows the comparison between the observation and simulated $PM_{2.5}$ concentrations. Both indicate that $PM_{2.5}$ concentrations were higher on the morning of March 19 than on the morning of March 20, and the observation and model values are almost the same. Comparisons between observation and simulation around J-ALPS sites indicate that the SCALE-Chem simulation could be used in further analyses of the impact of topography on aerosols.

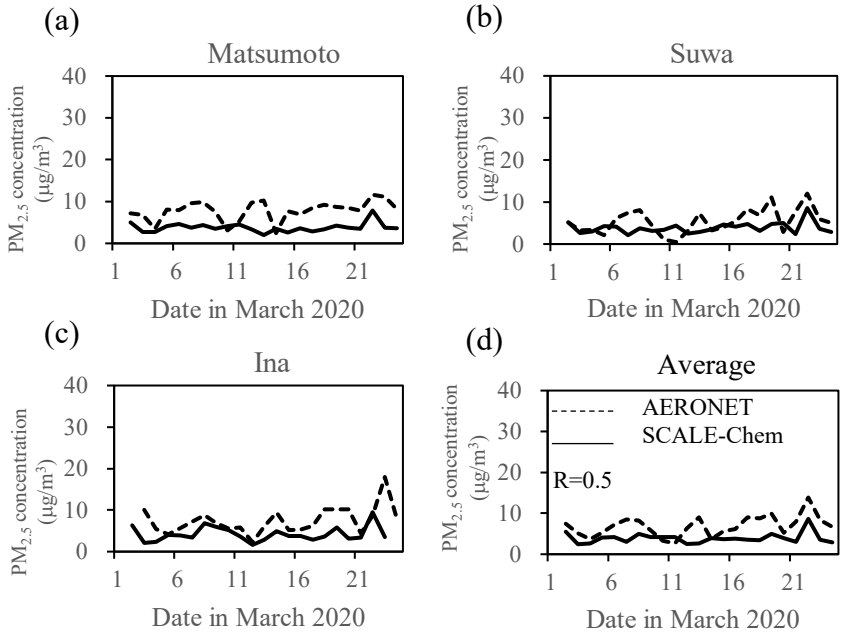

Figure 3. Daily mean $PM_{2.5}$ at (a) Matsumoto, (b) Suwa, and (c) Ina sites and (d) average of 3 sites in March 2020. The dashed line indicates Atmospheric Environmental Regional Observation System (AEROS) data, and the solid line indicates SCALE-chem simulation.

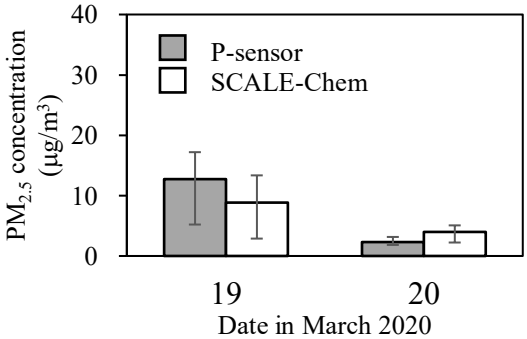

Figure 4. Observation $PM_{2.5}$ concentration and simulated $PM_{2.5}$ concentration by SCALE-Chem in the Ina basin on March 19 and 20, 2020, averaged from 06:00 to 10:00 local time. Error bars indicate the width of the maximum and the minimum values over average time.

296 **4 Feasible experiments using SCALE-Chem**

297 4.1 Mountain and local emission effects at J-ALPS sites

298 The mountain effects (*Mt effect*) on aerosols around J-ALPS sites could be investigated with the
299 differences between the control experiment (E1) and the experiment without topography (E2) as:
300
301 $Mt\ effect = (A_{E1} - A_{E2}) / A_{E1},$ (1)
302
303 where A_{Ex} indicates the value simulated by the experiment of Ex. Next, to evaluate the impact of
304 aerosols originating from emissions in Nagano Prefecture, we compared an experiment in which
305 emissions in Nagano Prefecture were eliminated (E3) with the control experiment (E1). This term
306 will be used in this work to refer to the local emission effect (*local effect*).
307
308 $Local\ effect = (A_{E1} - A_{E3}) / A_{E1},$ (2)
309
310 Figure 5 presents the daily change in *the Mt effect* (dotted line graph) and *local effect* (yellow bar
311 graph) estimated from $PM_{2.5}$ concentrations at J-ALPS sites. This clearly shows that the *MT effect*
312 is not always negative. That is to say, some days, the mountain reduces the aerosol concentrations,
313 and some days, it increases them. Hakuba was the most northerly of the seven sites. Here, the rate
314 of decrease in aerosol concentration due to the *Mt effect* was the greatest among the seven sites.
315 On days when there is a significant decrease in concentration due to the *Mt effect*, the wind
316 direction is often west to west-northwest. However, on days when aerosol concentrations are
317 increasing due to the *Mt effect*, the *local effect* can be seen. In Omachi, which is located next to
318 Hakuba to the north, the daily changes in the *Mt* and *local effects* are similar to those in Hakuba.
319 It was observed that the southwest wind tended to dominate on days when the rate of decrease due
320 to the *Mt effect* was high. In addition, as in Hakuba, the period of increased concentration due to
321 the *Mt effect* in early March seems to correspond to the period when the *local effect* is large.
322 Matsumoto has a smaller percentage of decrease in concentration due to the *Mt effect* than Hakuba
323 and Omachi. Suwa shows similar daily changes in the *Mt effect* and *local effect* as Matsumoto.
324 Minowa and Ina are geographically close, and the changes in the *Mt* and *local effects* are similar.
325 Iida, the most southerly of the seven sites, shows similar daily changes in *Mt effect* as Minowa and
326 Ina, but with a lower rate of decrease. The average of the seven sites shows that the rate of decrease
327 in aerosol concentration due to the *Mt effect* is greater than the rate of increase in aerosol
328 concentration due to the *Mt effect*. In addition, the *Mt effect* tends to have a positive value on the
329 day when the *local effect* is more prominent. This suggests that on days when the aerosol
330 concentration decreases due to the *Mt effect*, the effect of the mountains blocking the particles from
331 outside the prefecture is significant. On the other hand, the days when the aerosol concentration
332 increases due to the *Mt effect* are the days when air pollution caused by particles originating from
333 sources within the prefecture is likely to occur, so it can be inferred that the terrain effect amplifies
334 the concentration of particles originating from within the prefecture. The daily variation of the two
335 effects suggests that, even on days when the *local effect* is substantial, the *Mt effect* has a negative
336 value if the effect of stopping the inflow from outside the prefecture is greater than that of
337 increasing $PM_{2.5}$ concentration by the *local effect*.
338 As shown in Fig. 5, the *Mt effect* had a marked negative value on March 20 and a positive
339 value on March 9. In the next section, using March 20 and 9 as examples, we will examine the

aerosol distribution on a day when advection from outside is blocked by mountains and a day when mountains increase the concentrations, respectively.

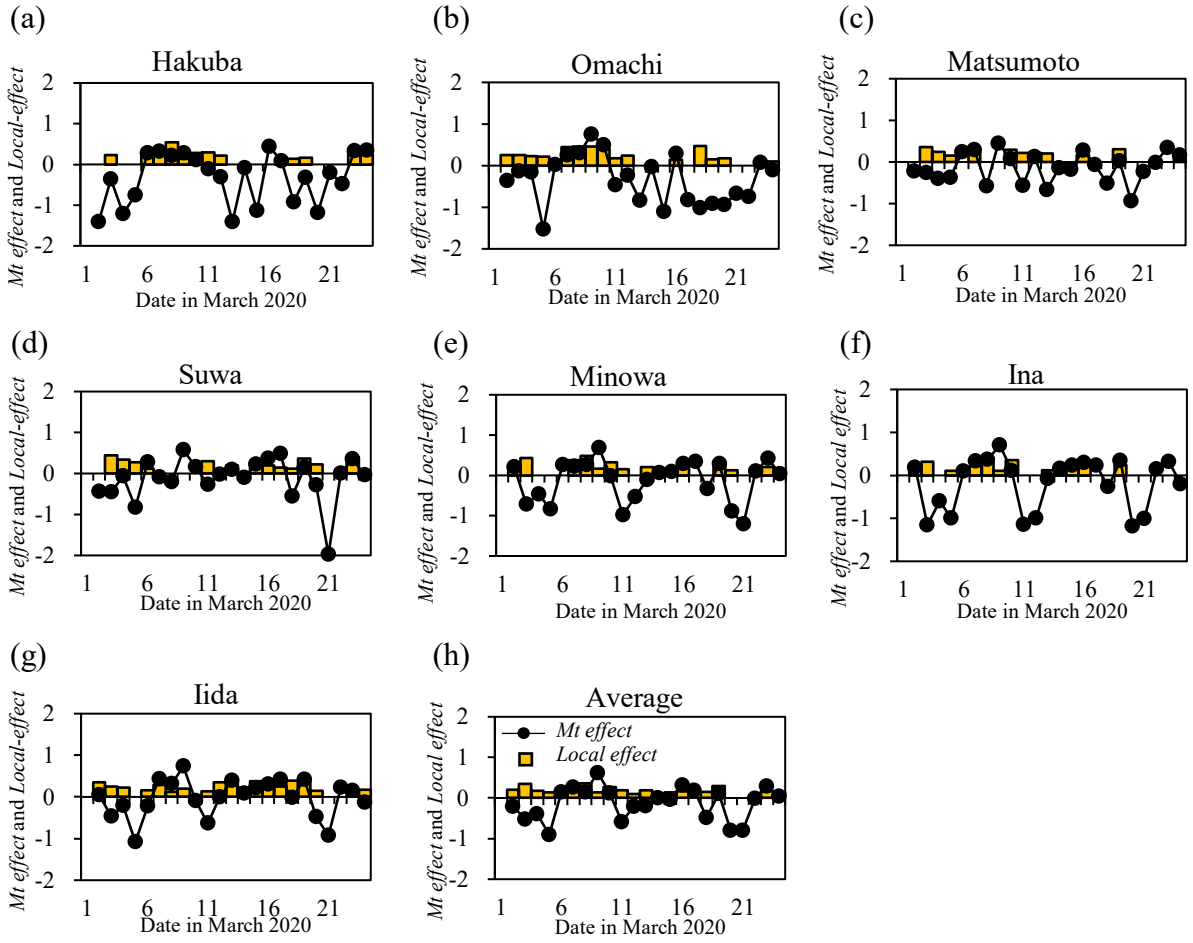

Figure 5. Daily change of *Mt effect* (dots line graph) and *Local effect* (yellow bar graph) estimated from $PM_{2.5}$ concentrations at J-ALPS sites in March 2020. The *Local effect* is a graph showing days when the value was greater than 0.1.

4.2 Mechanisms of the mountain effect on aerosols

First, the 20th of March, as shown in Fig. 4, was considered. Satellite observations and numerical model simulations show that aerosol concentrations are high from spring to summer over East Asia (Nakata et al., 2018). Spring is the season when aerosols from mainland China are especially likely to be transported to Japan (Nakata et al., 2015). Figure 6 shows the distribution of the $PM_{2.5}$ concentration simulated by SCALE-Chem on March 20, from 6:00 to 10:00 local time. The upper figures represent the case of the E1 experiment and the lower E2 experiment. Transboundary pollution that had crossed the Sea of Japan was also observed. However, the $PM_{2.5}$ concentrations were low around the J-ALPS sites on March 20. It can be seen that the $PM_{2.5}$ air advection is blocked by the mountains. The results of E2, simulated without mountains, show that particles transported from the west also flow into Nagano Prefecture. Comparing the results of the

E1 and E2 simulations, it is clear that the mountain effect reduces air pollution in the vicinity of the J-ALPS site.

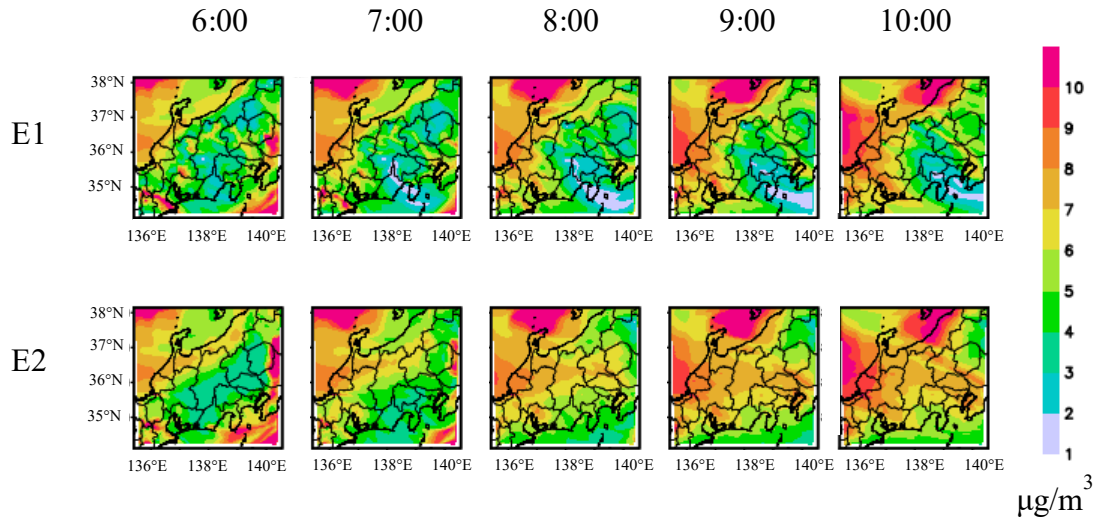

Figure 6. Distribution of $PM_{2.5}$ concentrations by SCALE-Chem from 06:00 to 10:00 local time on March 20, 2020. The upper and the lower figures represent the E1 and E2 experiments, respectively.

Figure 7 (a) and (b) show the 2-dimensional distribution of $PM_{2.5}$ and wind vectors denoted by black arrows from SCALE-Chem simulations in two cases of experiment E1 and E2 over Nagano Prefecture. It is clear that the $PM_{2.5}$ concentrations (represented with the color scale) are higher in E2 than in E1. Figures 7(c), 7(d), and 7(e) show the vertical distribution of $PM_{2.5}$ in a cross-sectional view in the east-west direction at 36.5°, 36, and 35.5°N, respectively. This shows that aerosol particles are being held back by the mountains. On March 20, the prevailing wind was from the west, and we can assume that aerosol particles transported from this direction were blocked by mountains on the west side. To examine the extent to which $PM_{2.5}$ concentrations changed due to the effect of mountains, the east-west cross-sections of the mountain effect calculated by equation (1) are shown in Figs.7 (f)–(g). Near Omachi at 36.5° °N, it is clear that aerosols are held back by the mountains to the west. In the vicinity of Suwa at 36°N, there is a chain of mountains to the west, although their elevation is lower than in the vicinity of Omachi, and it can be seen that these mountains are still capable of blocking aerosols. The Iida site is near 35.5°N, and the elevation of the mountains on the west side is lower than that near 36.5°N; however, the effect of the mountains on the west side still reduces the aerosol concentration. In addition, the vertical cross-section shows that the aerosol concentration in the upper layer increases as the concentration in the lower layer decreases, owing to the mountain effect. On March 20, the air was clear when we observed it in the Ina Basin, but if the mountains were not effective in preventing aerosols from the outside, it is likely that the aerosol concentration would have increased due to transboundary pollution.

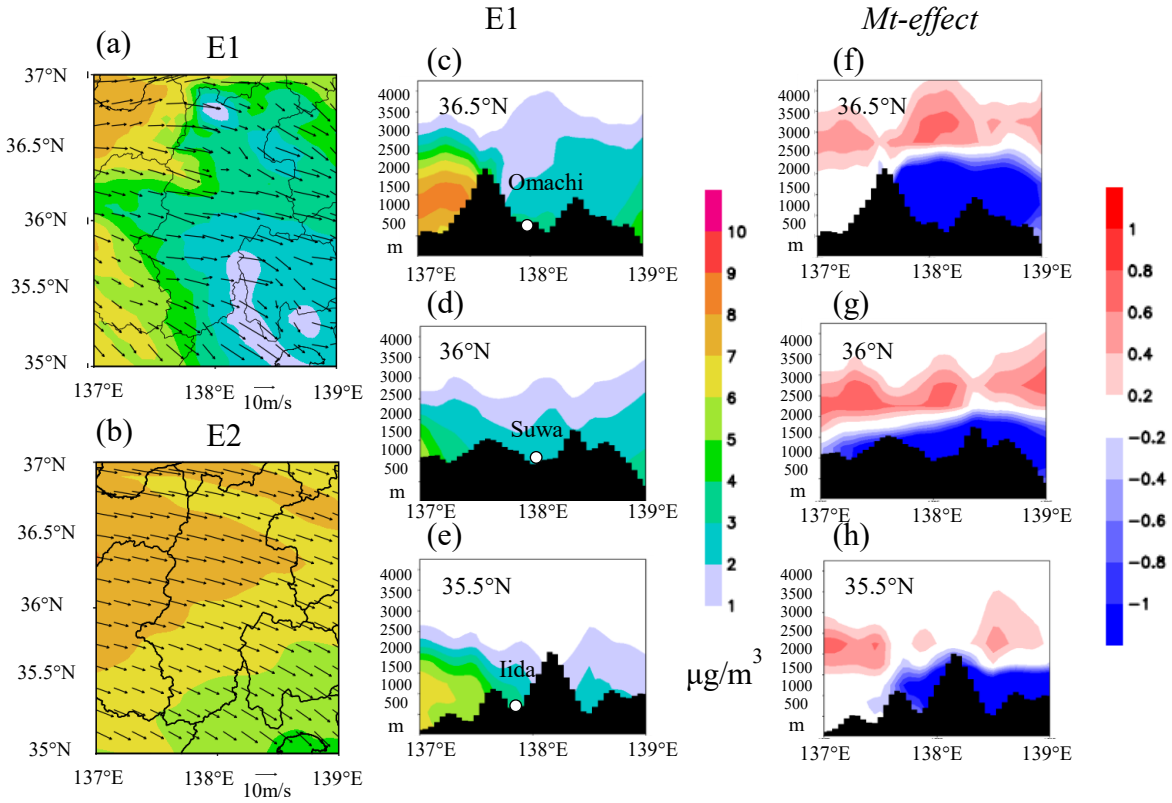

Figure 7. Two-dimensional distribution of $PM_{2.5}$ concentrations (presented with the color scale in the middle) and wind vectors (denoted by black arrows) from SCALE-Chem simulations in two cases of experiment (a) E1 and (b) E2. Figures (c), (d), and (e) present the vertical distribution of $PM_{2.5}$ concentrations for experiment E1 in a cross-sectional view in the east-west direction at 36.5°N, 36°N, and 35.5°N, respectively. The *Mt effect* is shown in the right side figures (f), (g), and (h); scaled color is shown to the far right. Averaged from 06:00 to 10:00 local time on March 20, 2020.

Below is a summary of the study results on the days when aerosol concentrations increased due to the *Mt effect*. March 9 was a day when the *Mt effect* was positive at all seven sites, as shown in Figure 5. Figures 8(a) and 8(b) show the $PM_{2.5}$ concentration distribution and wind vectors around Nagano Prefecture on March 9 for the E1 and E2 simulations, as shown in Fig. 7. Compared with the case of March 20 shown in Fig. 7, Fig. 8 on March 9 indicates that the wind was weaker and the $PM_{2.5}$ concentrations were higher in the basin. However, the simulation without topography showed that $PM_{2.5}$ concentrations were uniformly distributed throughout Nagano Prefecture on March 9. This suggests that the concentrations were increasing in Nagano Prefecture due to topographical effects. The east-west cross-sectional view presented in Figs. 8(c)–(e) shows that the aerosol particle concentration was higher between the mountains. Figures 8 (f) to (g) present the concentration change due to the mountain effect. The *Mt effect* demonstrates an increase in aerosol concentration in the lower layer. Topographical effects have been shown to enhance air pollution in basins (Zhang et al., 2019). This is thought to be related to the fact that on days when the effect of local emissions is strong, the effect of mountains is positive. On days when

aerosol concentrations increase due to emission sources within the prefecture, the topographical effect of the basin reinforces the increase in concentrations over the J-ALPS sites. The vertical distribution of temperature at J-ALPS sites at 6:00 local time on March 9, when the aerosol concentration increased due to the positive *Mt effect*, is shown in Fig. 9. In the early morning of March 9, the ground was cooler, and a ground inversion layer formed. This is thought to have caused the aerosol concentration to rise because the atmosphere near the ground surface became stable, making it difficult for particles to diffuse in the upper layer. In the simulation without surrounding mountains (E2), the temperature near the ground was not as low as in the control simulation (E1), so the inversion layer was not as thick as in E1. This suggests that on days when the *Mt effect* is positive, the weather conditions are conducive to the accumulation of aerosols in the lower atmosphere. As can be seen from Fig. 5, there is a relationship between the positive *Mt effect* and *local effect*. The positive *Mt effect* increases the concentration of particles near the surface owing to the effect of topography. This effect is more pronounced when there is a *local effect*. On the other hand, if the inversion layer is caused by the topography effect, the particles brought from the outside will not increase the concentration near the surface. Therefore, there is no correlation between the *local effect* and the negative *Mt effect*. On March 19, when observations were made in the Ina Basin, atmospheric turbidity was observed in the morning, which is thought to have been caused by the positive *Mt effect*. The *Mt effect* was also positive on March 22, when the observed AOT and $PM_{2.5}$ concentrations were high for the period, suggesting that the positive *Mt effect* may have accelerated the concentration increase.

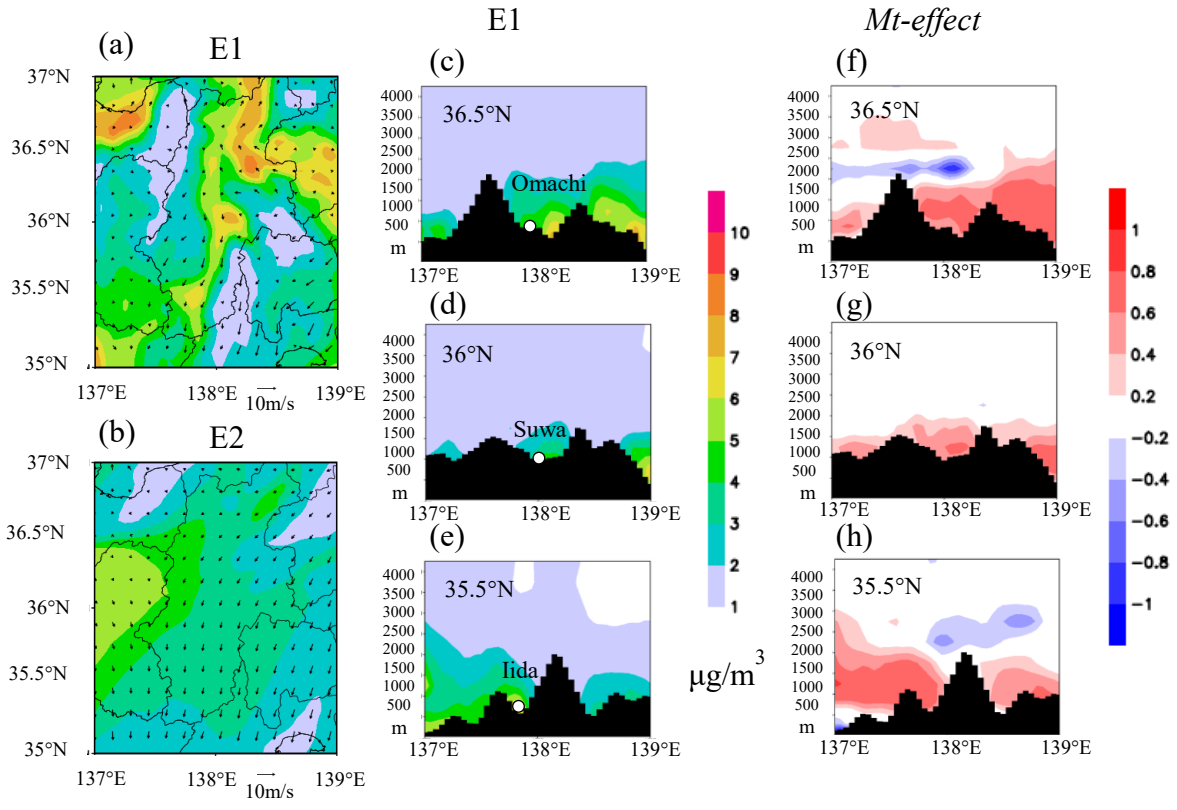

Figure 8. The same as Fig.7, but for March 9, 2020.

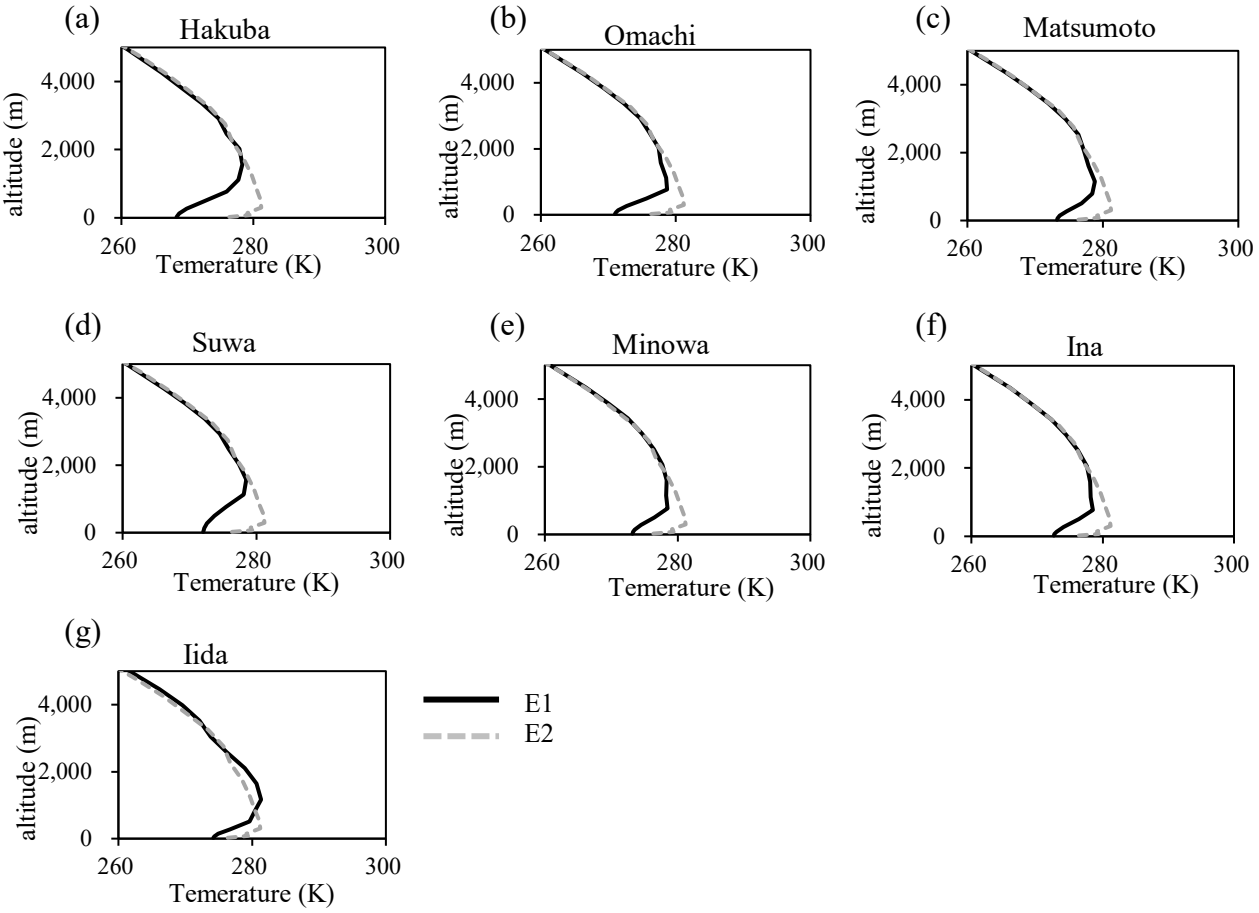

Figure 9. Vertical distribution of temperature at 06:00 local time on March 9, 2020, at (a) Hakuba, (b) Oamachi, (c)Matsumoto, (d) Suwa, (e) Minowa, and (f) Iida sites simulated by SCALE-Chem for E1 and E2.

4.3 Simulation results over J-ALPS

Figure 10 (a) shows the distribution of the *Mt effect* averaged during the simulation period, and it can be seen that the *Mt effect* is negative over the J-ALPS sites. Thus, it appears that mountains have a blocking effect on polluting particles from the outside. However, aerosol concentrations are not only reduced but sometimes increased by the presence of mountains. Figure 10(b) shows the distribution of the *local effect* in Nagano Prefecture, and it can be seen that the distribution corresponds to the distribution of areas where the negative *Mt effect* is relatively small. The positive *Mt effect* on aerosol concentrations can also be described as the effect of increasing pollutant concentrations in basins. In areas where the *local effect* is large, the positive *Mt effect* is stronger. On days when there is no advection from outside the prefecture, and the increase in concentration due to emissions within the prefecture is dominant, the concentration will increase because of the positive *Mt effect*. Figure 10 shows the average for the period, so the negative *Mt effect* is lower in areas where the *local effect* is large. Negative and positive *Mt effects* are thought to occur simultaneously, but the averaged results indicate that the negative effect is significant. The simulation results show that the *Mt effect* blocking transboundary pollutant particles from

outside was greater than the enhancement of local air pollution due to the topographical effects over the J-ALPS sites in March 2020.

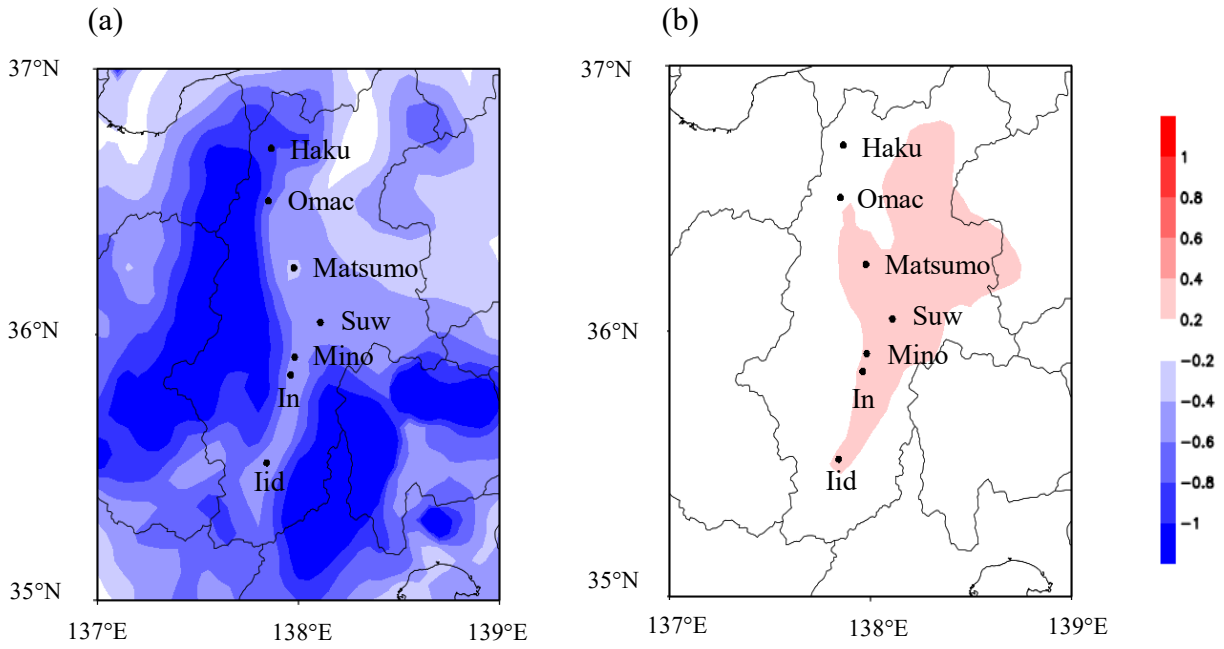

Figure 10. Distribution of (a) *Mt effect* and (b) *Local effect* averaged during simulation period.

To examine the frequency of days with negative and positive *Mt effects*, Fig. 11 shows the rate of occurrence days at each J-ALPS site. The days when the *Mt effect* reaches values greater than +0.1 are considered 'positive *Mt effect*,' those less than -0.1 'negative *Mt effect*,' and others when the absolute value of the *Mt effect* is less than 0.1 are classified as having 'no effect.' As shown in Fig. 11, Hakuba, Omachi, and Matsumoto, in the northern part of the J-ALPS sites, have a negative *Mt effect* rate higher than 50%. In other words, mountains blocked the aerosol particles more than half the time. In March, transboundary pollution aerosols were transported from mainland China. This area has high mountains to the west, and hence, the pollutant aerosols seem to be blocked by the *Mt effect*. On the other hand, Iida, Ina, and Minowa, which are located in the southern part of the sites, tended to have a higher percentage of days with a positive *Mt effect*.

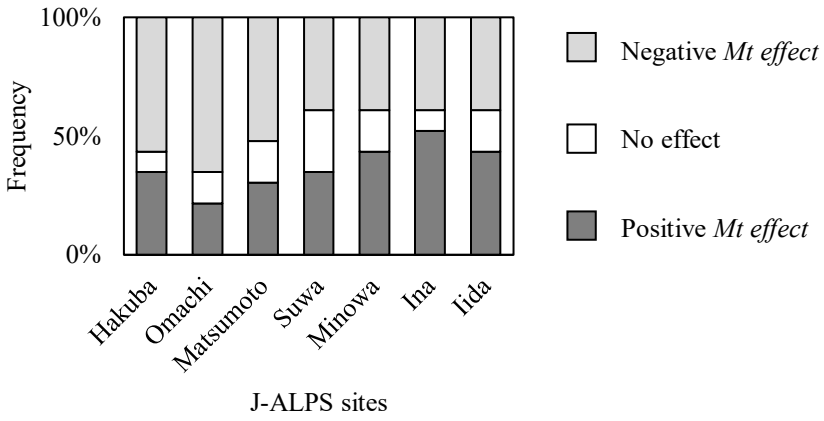

Figure 11. Frequency of days with positive *Mt effect* and days with negative *Mt effect* during simulation period at each site.

Figure 12 shows the relative daily frequency of the positive and negative Mt effects at each J-ALPS site in March 2020. The sunrise and sunset are around 6:00 and 18:00, respectively, at a local time in March in Nagano Prefecture. In Hakuba, there is a distinct diurnal variation in which a positive *Mt effect* is more likely to occur before sunrise and at night, and the frequency of positive *Mt effect* is lower during the day. During the hours when a positive *Mt effect* is more likely to occur, the frequency of negative *Mt effect* is relatively lower, but the percentage of negative *Mt effect* occurring throughout the day is high, reaching approximately 80% during the day. In Omachi, the frequency of the *Mt effect* showed diurnal variation, with a higher percentage of positive *Mt effect* occurring around sunrise and at night. However, during other times of the day, the percentage of the negative *Mt effect* was high. In Matsumoto, the percentage of the *Mt effect* was also high, but the percentage of the positive *Mt effect* tended to be higher around sunrise and at night. In Suwa and Minowa, there was no apparent diurnal variation, but the highest percentage of positive *Mt effect* was observed at 04:00. In Ina and Iida, the percentage of the positive *Mt effect* tends to be higher in the early morning than in the daytime. At the J-ALPS site, a negative *Mt effect* dominates at all times of day, but a positive *Mt effect* tends to happen in the early morning when an inversion layer is more likely to occur.

It was found that mountains have a two-way effect, preventing advection from the outside and trapping air masses in the basin surrounded by mountains. The effects are greater depending on the meteorological conditions, the presence or absence of external transboundary pollution, and the level of local emissions.

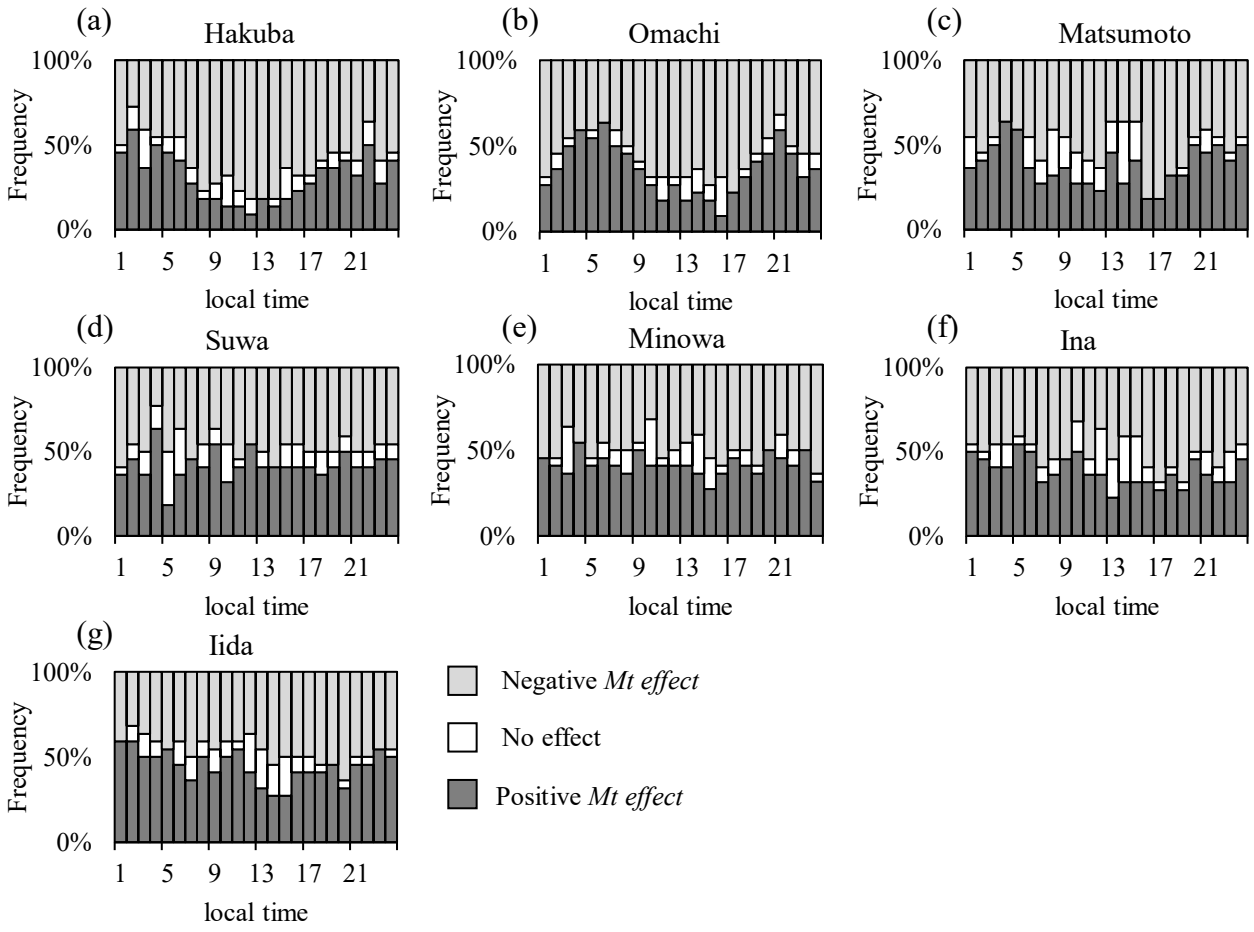

Figure 12 Time variation of frequency in positive *Mt effect* and negative *Mt effect* during simulation period at each site.

5 Conclusions

To investigate the effect of mountain topography on aerosols, intensive DRAGON/J-ALPS observations were conducted around Nagano Prefecture, Japan. High concentrations of aerosol pollution were not observed in March 2020. To interpret the measurements of DRAGON/J-ALPS, three types of simulation experiments were carried out using a regional chemical transport model, SCALE-Chem. One was the control simulation, the second was the simulation without topography, and the third was the simulation eliminating local emissions in Nagano Prefecture. From the results of these simulations, we estimated the *Mt* and *local effects* in Nagano Prefecture. The presence of mountains was found to increase or decrease aerosol concentration in some cases. However, when averaged over the simulation period, the results show that the *Mt effect* effectively reduces aerosol concentrations. On the days when aerosol concentrations increased due to the *Mt effect*, meteorological conditions with high local emissions and the basin effect acted synergistically to accelerate the increase in aerosol concentrations. This trend was more pronounced in the southern region of the J-ALPS. However, at all sites, the aerosol inflow was blocked by mountains located to the west.

In Japan, spring is the season when transboundary pollution from mainland China is most likely to be observed, but the aerosols from outside were suppressed at the J-ALPS sites because they are surrounded by high mountains. Therefore, even on days when transboundary pollution was observed in other parts of Japan, the aerosol concentrations were not very high at the J-ALPS sites. In future work, we would like to investigate the seasonal variation of the mountain effect using the data observed from seasons other than spring. Furthermore, the magnitude of transboundary pollution, advection height, and the influence of meteorological conditions should be taken into account, along with topographical effects.

Acknowledgments

The authors would like to thank Dr. Brent Holben & NASA/AERONET group, and Prof. Itaru Sano and local organization members of J-ALPS. This study was supported in part by the Global Change Observation Mission - Climate project by JAXA (no. JX-PSPC – 524344 & 530188), JSPS KAKENHI Grant Number 19h04242. Yousuke Sato was supported by the Research Field of Hokkaido Weather Forecast and Technology Development (Hokkaido Weather Technology Center Co. Ltd.). SCALE was developed by Team-SCALE of RIKEN (https://scale.riken.jp/). The SCALE source code is downloadable from the SCALE website (https://scale.riken.jp/). The chemical model part of SCALE-Chem is subject to a license agreement with the Japan Meteorological Agency. Further information is available at https://www.mri-jma.go.jp/Dep/glb/nhmchem_model/application_en.html. The AOT data at the J-ALPS site are available at AERONET via https://aeronet.gsfc.nasa.gov/). The $PM_{2.5}$ data used in this study are available at AEROS via (http://soramame.taiki.go.jp/).

References

Aikawa, M., Ohara, T., Hiraki, T., Oishi, O., Tsuji, A., Yamagami, M., et al. (2010), Significant geographic gradients in particulate sulfate over Japan determined from multiple-site measurements and a chemical transport model: Impacts of transboundary pollution from the Asian continent. *Atmospheric Environment*, *44*(3), 381–391, doi:10.1016/j.atmosenv.2009.10.025.

Chang, Y.S., Carmichael, G. R., Kurita, H., & Ueda, H. (1989), The transport and formation of photochemical oxidants in central Japan. *Atmospheric Environment*, *23*(2), 363–393.

Chuang, M., Chiang, P., Chan, C., Wang , C., Chang, E., & Lee, C. (2008), Elevated 3D structures of PM2.5 and impact of complex terrain-forcing circulations on heavy haze pollution over Sichuan Basin, China. *Science of the Total Environment*, *399*, 128–146.

Diémoz, H., Barnaba, F., Magri, T., Pession, G., Dionisi, D., Pittavino, S., et al. (2019), Transport of Po Valley aerosol pollution to the northwestern Alps –Part 1: Phenomenology. *Atmospheric Chemistry and Physics, 19*, 3065–3095, https:doi.org/10.5194/acp-19-3065-2019.

Giglio, L., Randerson, J. T., van der Werf, G. R., Kasibhatla, P. S., Collatz, G. J., Morton, D. C. & DeFries, R. S. (2010), Assessing variability and long-term trends in burned area by merging multiple satellite fire products, *Biogeosciences*, *7*, 1171–1186.

Giles, D. M., Sinyuk, A., Sorokin, M. G., Schafer, J. S., Smirnov, A., Slutsker, I., et al. (2019), Advancements in the Aerosol Robotic Network (AERONET) Version 3 database – automated near-real-time quality control algorithm with improved cloud screening for Sun photometer aerosol optical depth (AOD) measurements. *Atmospheric Measurement Techniques*, *12*, 169–209, https://doi.org/10.5194/amt-12-169-2019.

Guenther, A., Karl, T., Harley, P., Wiedinmyer, C., Palmer, P. I., & Geron, C. (2006), Estimates of global terrestrial isoprene emissions using MEGAN (Model of Emissions of Gases and Aerosols from Nature). *Atmospheric Chemistry and Physics*, *6*, 3181–3210.

Holben, B.N., Eck, T.F, Slutsker, I., Tanré, D., Buis, J.P., Setzer, A., et al. (1998), AERONET - A federated instrumentnetwork and data archive for aerosol characterization. *Remote Sensing of Environment*, *66,* 1–16.

Holben, B. N., Kim, J., Sano, I., Mukai, S., Eck, T. F., Giles, D. M., et al. (2018), An overview of meso-scale aerosol processes, comparison and validation studies from DRAGON networks. *Atmospheric Chemistry and Physics*, *18* (2), 655–671.

Hu, W., Zhao, T., Bai, Y., Shen, L., Sun, X., & Gu, Y. (2020), Contribution of regional PM2.5 transport to air pollution enhanced by sub-basin topography: A modeling case over Central China. *Atmosphere*, *11*(11), 1258, https://doi.org/10.3390/atmos11111258.

Inatsu, M., Tanji, S., & Sato, Y. (2020), Toward predicting expressway closures due to blowing snow events. Cold Regions Science and Technology, *177*, 103123.

IPCC (Intergovernmental panel on climate change) (2013), Climate change: The Physical Science Basis, Contribution of Working Group 1 to the Fifth Assessment Report of the IPCC, Cambridge University Press, Cambrige.

Kajino, M., Deushi, M., Sekiyama, TT., Oshima, N., Yumimoto, K., Tanaka, TY., et al. (2019), NHM-Chem, the Japan meteorological agency's regional meteorology – chemistry model: Model evaluations toward the consistent predictions of the chemical, physical, and optical properties of aerosols. *Journal of the Meteorological Society of Japan*, *97*(2), 337–374.

Kajino, M., Deushi, M., Sekiyama, T. T., Oshima, N., Yumimoto, K., Tanaka, T. Y., et al. (2021), Comparison of three aerosol representations of NHM-Chem (v1.0) for the simulations of air quality and climate-relevant variables. *Geoscientific Model Development,* https://doi.org/10.5194/gmd-14-2235-2021.

Kaneyasu, N., Yamamoto, S., Sato, K., Takami, A., Hayashi, M., Hara, K., et al. (2014), Impact of long-range transport of aerosols on the PM2.5 composition at a major metropolitan area in the northern Kyushu area of Japan. *Atmospheric Environment*, *97*, 416–425, doi:10.1016/J.ATMOSENV.2014.01.029.

Kurokawa, J., Ohara, T., Morikawa, T., Hanayama, S., Janssens-Maenhout, G., Fukui, T., et al. (2013), Emissions of air pollutants and greenhouse gases over Asian regions during 2000–2008:

614 Regional Emission inventory in Asia (REAS) version 2. *Atmospheric Chemistry and Physics*, *13*,
615 11019–11058.
616
617 Li, M., Zhang, Q., Kurokawa, J., Woo, J.-H., He, K., Lu, Z., et al. (2017), MIX: A mosaic Asian
618 anthropogenic emission inventory under the international collaboration framework of the MICS-
619 Asia and HTAP. *Atmospheric Chemistry and Physics*, *17*, 935–963.
620
621 Nakata, M., Sano, I., Mukai, S., & Holben, B. N. (2013), Spatial and Temporal Variations of
622 Atmospheric Aerosol in Osaka. *Atmosphere*, *4*(2), 157–168, doi:10.3390/atmos4020157.
623
624 Nakata, M, Sano, I., & Mukai, S. (2015), Air Pollutants in Osaka (Japan). *Frontiers in*
625 *Environmental Science*, *3*, 18, doi: 10.3389 /fenvs.2015.00018.
626
627 Nakata, M., Mukai, S., & Yasumoto, M. (2018), Seasonal and regional characteristics of aerosol
628 pollution in East and Southeast Asia. *Frontiers in Environmental Science*, *6*, 29,
629 https://doi.org/10.3389/fenvs.2018.00029.
630
631 Nishizawa, S., Yashiro, H., Sato, Y., Miyamoto, Y., & Tomita, H. (2015), Influence of grid
632 aspect ratio on planetary boundary layer turbulence in large-eddy simulations. *Geoscientific*
633 *Model Development, 28*, 8(10), 3393–341.
634
635 Togashi, H. (2001), Geomorphology and geology of Nagano prefecture. *Bulletin of Nagano*
636 *Nature Conservation Research Institute*, *4*(1), 1–9 (in Japanese).
637
638 Sano, I., Mukai, S., Nakata, M., & Holben, B. N. (2016), Regional and local variations in
639 atmospheric aerosols using ground-based sun photometry during distributed regional aerosol
640 gridded observation networks (DRAGON) in 2012. *Atmospheric Chemistry and Physics*, *16*,
641 14795–14803, doi:10.5194/acp-16-14795-2016.
642
643 Sasaki, K., Kurita, H., Carmichael, G. R., Chang, Y. S., Murano, K., & Ueda, H. (1988),
644 Behavior of sulfate, nitrate and other pollutants in the long-range transport of air pollution.
645 *Atmospheric Environment*, *22*(7), 1301–1308.
646
647 Sato, Y., Nishizawa, S., Yashiro, H., Miyamoto, Y., Kajikawa, Y., & Tomita, H. (2015), Impacts
648 of cloud microphysics on trade wind cumulus: which cloud microphysics processes contribute to
649 the diversity in a large eddy simulation? *Progress in Earth and Planetary Science, 2*(1), 23,
650 doi:10.1186/s40645-015-0053-6.
651
652 Snider, G., Weagle, C. L., Murdymootoo, K. K., Ring, A., Ritchie, Y., Stone, E., et al. (2016),
653 Variation in global chemical composition of PM2.5: emerging results from SPARTAN.
654 *Atmospheric Chemistry and Physics*, *16,* 9629–9653, doi:10.5194/acp-16-9629-2016.
655
656 Su, B., Li, H., Zhang, M., Bilar, M., Wang, M., Atique, L., et al. (2020), Optical and physical
657 characteristics of aerosol vertical layers over Northeastern China. *Atmosphere*, *11*, 501.
658

Van Donkelaar, A., Martin, R. V, Brauer, M., & Boys, B. L. (2015), Use of satellite observations for long-term exposure assessment of global concentrations of fine particulate matter. *Environmental Health Perspectives*, *123*, 135–143, doi:10.1289/ehp.1408646.

Zhang, Z., Xu, X., Qiao, L., Gong, D., Kim, S. J., Wang, Y., & Mao, R. (2018), Numerical simulations of the effects of regional topography on haze pollution in Beijing. *Scientific Reports*, *8*, 5504.

Zhang, L. Guo, X. Zhao, T., Gong, S., Xu, X., Li, Y., et al. (2019), A modelling study of the terrain effects on haze pollution in the Sichuan Basin, *Atmospheric Environment*, *196,* 77-85.